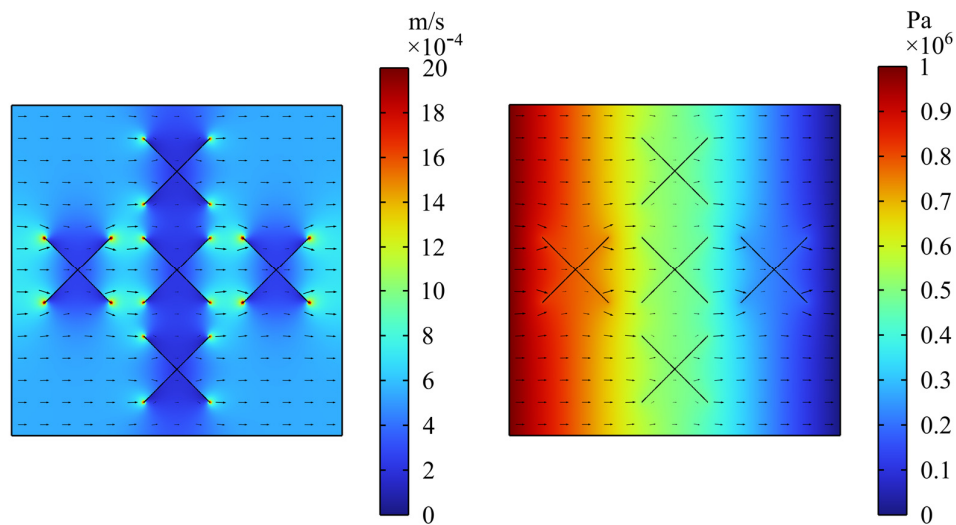


## Supplementary Materials

Fig. 1a displays Darcy velocity contours, affected by fractures. Darcy's Velocity increases at fracture endpoints and decreases at intersections. Arrows represent seepage flow direction and magnitude. Fig. 1b presents pore water pressure contours, relating to Darcy velocity. Fluid flows from matrix to fissure, accelerating and increasing pressure at endpoints. Pressure changes influence Darcy velocity. To study permeability sensitivity, pressure flow line and velocity field diagrams were combined.



**Figure S1. (a) Darcy velocity contour (b) Pore water pressure contour**

Fracture density significantly impacts Darcy velocity and pore water pressure in the rock matrix. Fig. 2 illustrates six models of permeability changes with varying fracture density. Models a-c show Darcy velocity changes, while models d-f display pore water pressure changes. Increased fracture density leads to more complex fluid movement. Model a highlights velocity changes on fracture surfaces, with acceleration at endpoints. Model b shows increased fluid velocity at the lower inlet and decreased at the upper part. Model c exhibits a more pronounced distribution of acceleration areas. Models d-f reveal that rapid pore water pressure changes concentrate in

high-flow regions, while water pressure decreases in low-flow areas.

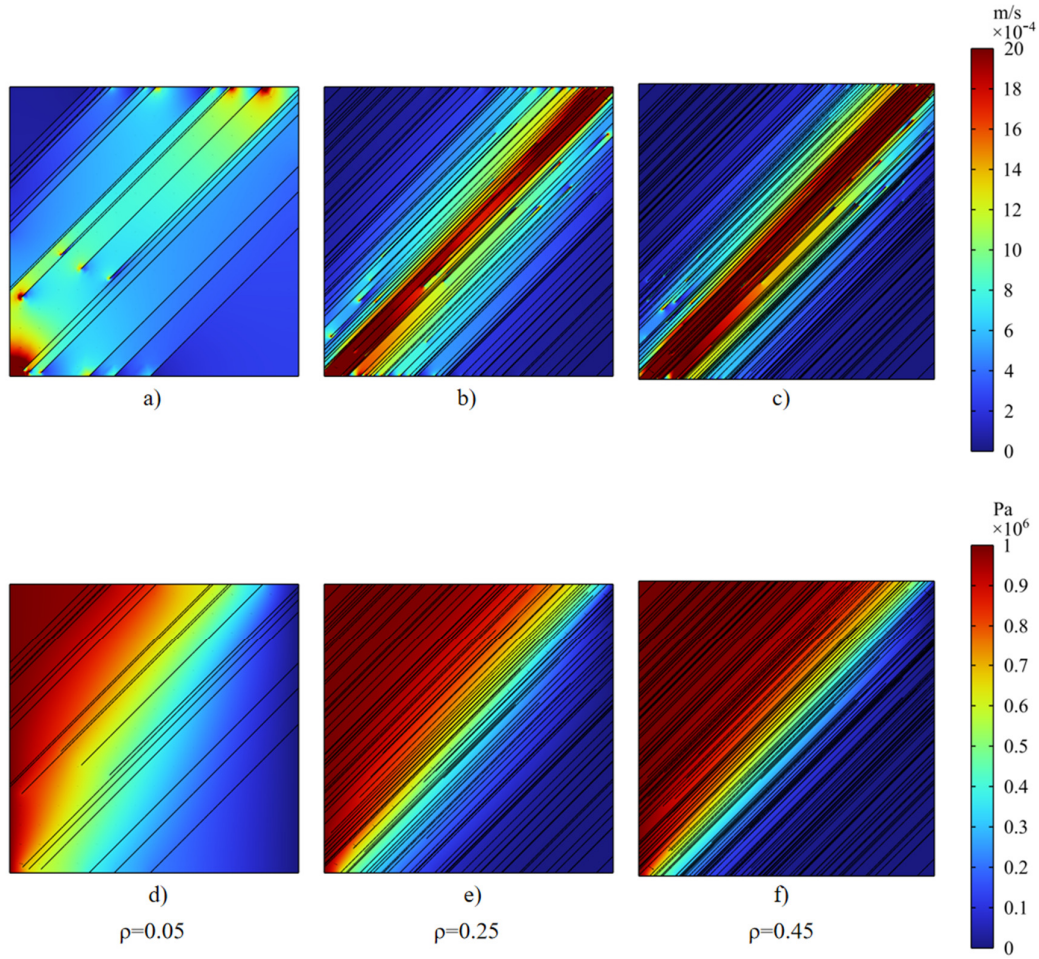


**Figure S2.** Effect of density on (a-c) Darcy's velocity and (d-f) pore water pressure

Fracture angle variations significantly impact Darcy velocity and pore water pressure in the rock mass matrix. Fig. S3 shows six models representing the influence of angle variation on permeability. Models a-c demonstrate angle impacts on Darcy velocity, while models d-f show pressure effects. Model a highlights velocity changes at fracture ends and even pressure distribution. Model b exhibits greater flow velocity in connected high hydraulic gradient regions and perpendicular pressure distribution. In Model c ( $90^\circ$  fracture angle), fluid seepage effects vanish, with no velocity changes and uniform pressure distribution in matrix seepage direction.

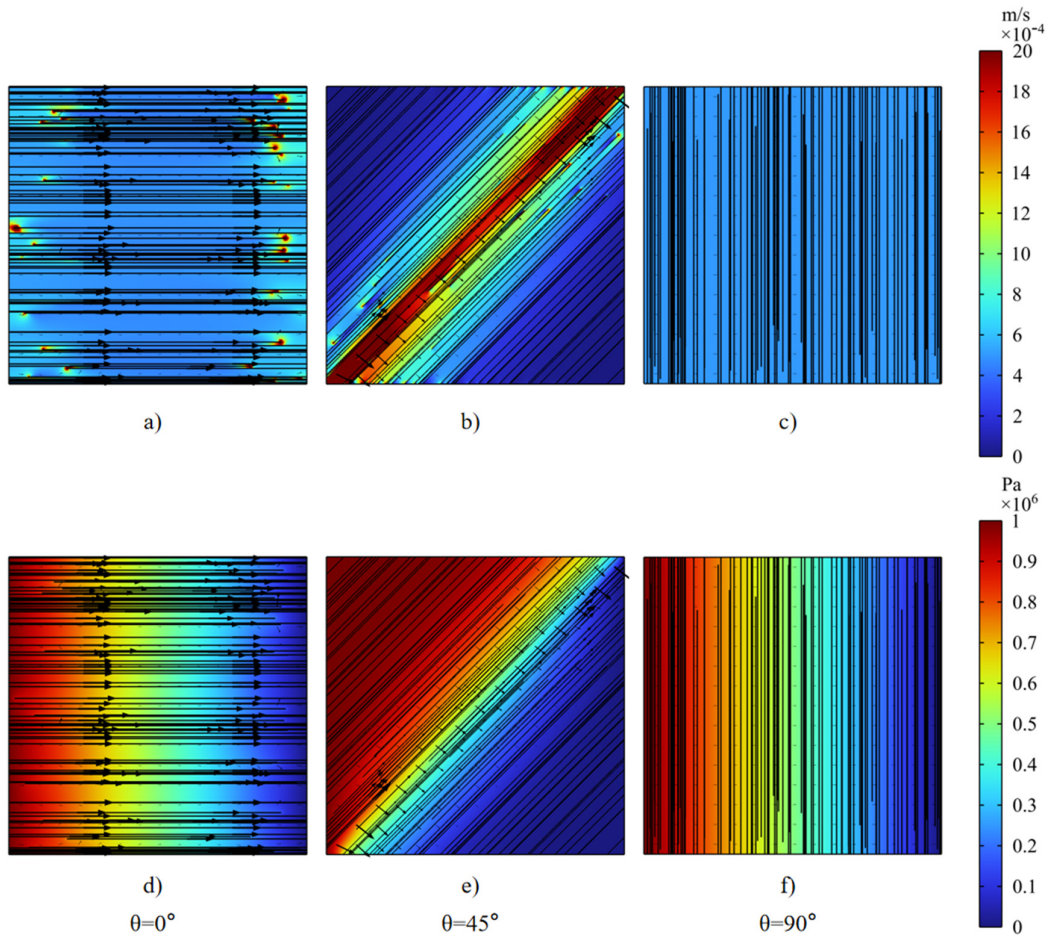


**Figure S3.** Effect of fracture direction on flow rate and water pressure

Fracture angle variations significantly impact Darcy velocity and pore water pressure in the rock mass matrix. Fig. S4 shows six models illustrating aperture variation effects on permeability. Models a-c display the impact on Darcy velocity, while models d-f show hydraulic pressure effects. From Model a to c, increasing aperture raises flow velocity in high hydraulic gradient zones and decreases it elsewhere. Pressure transmission changes substantially in high gradient regions, with pressure outside these zones decreasing and changes concentrating in regions with shifting high hydraulic gradients.

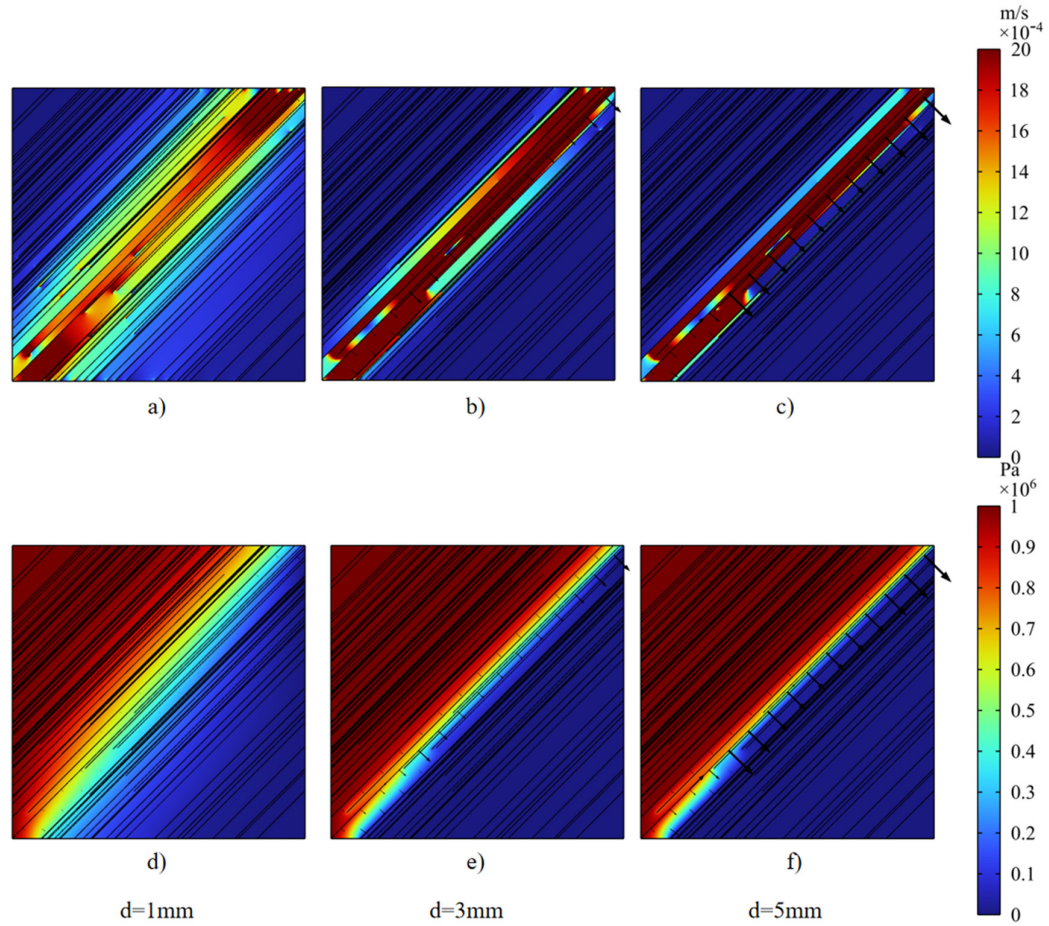


**Figure S4.** Effect of Aperture on flow rate and water pressure

Fracture length increase significantly impacts Darcy velocity and pore water pressure in the rock matrix. Fig. S5 displays six models illustrating fracture length effects on permeability. Models a-c show the impact on Darcy velocity, while models d-f display hydraulic pressure effects. As fracture length increases, fluid velocity in high hydraulic gradient regions at the lower inlet and upper outlet sides increases, shifting from dispersed to concentrated states. Darcy velocity decreases in other areas. Pressure and fracture length correlation is not significant.



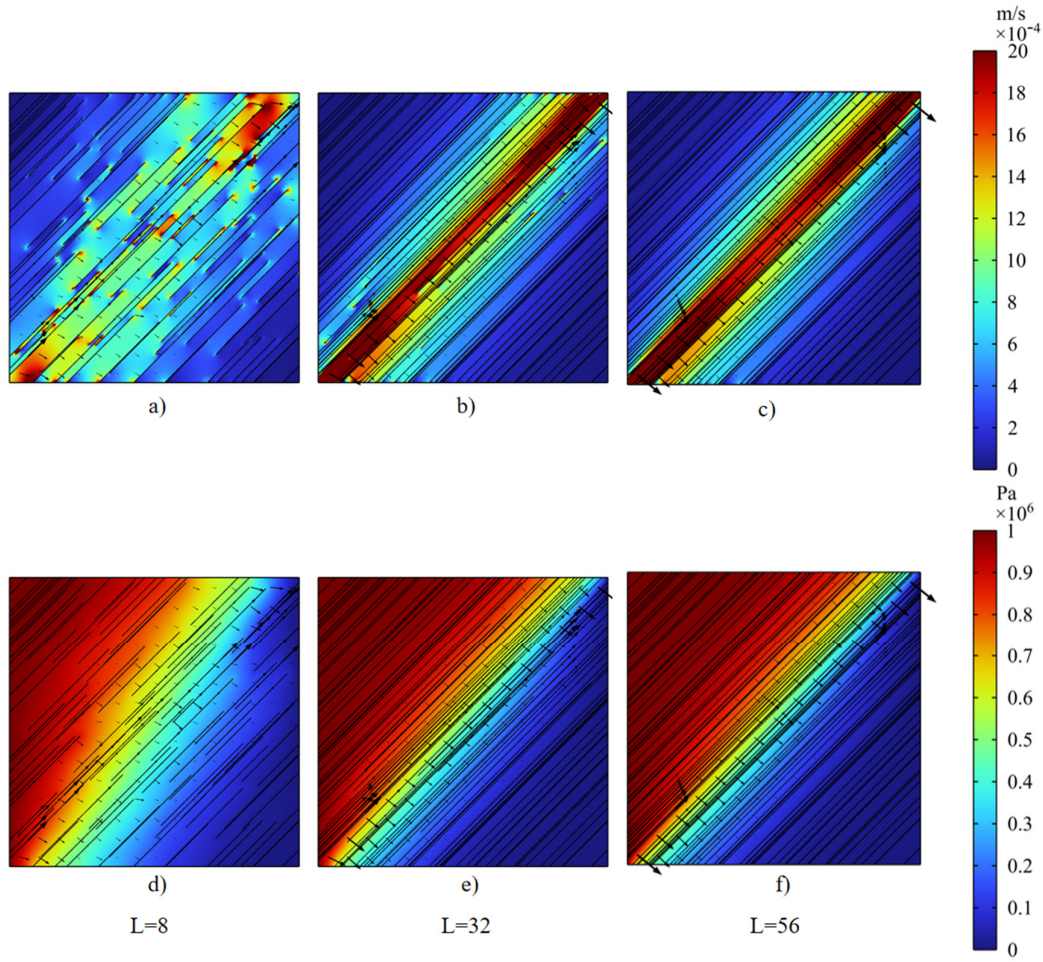


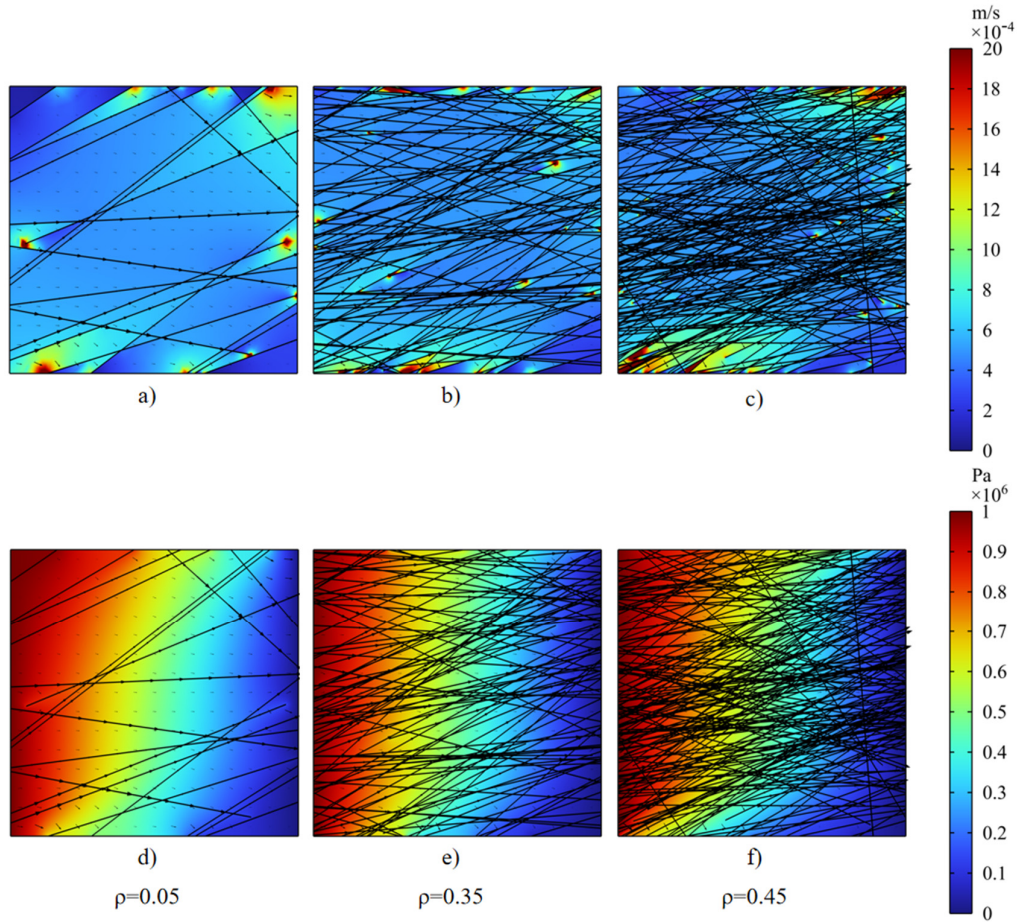
**Figure S5.** Effect of fracture length on flow rate and water pressure

Fracture density significantly impacts matrix Darcy velocity but not pore water pressure. Fig. S6 presents six models illustrating permeability effects with varying fracture densities. Models a-c show Darcy velocity changes with increasing density, while models d-f display pore water pressure variations. As fracture density increases, fluid movement in the rock mass shifts, matrix seepage decreases, fracture seepage increases, and individual fracture flow rates decrease. Models d-f reveal that increased fracture numbers don't significantly change matrix pressure distribution, and pore water pressure in individual fractures decreases.

two-dimensional random fracture network simulation experiment parameter design (Table S1).

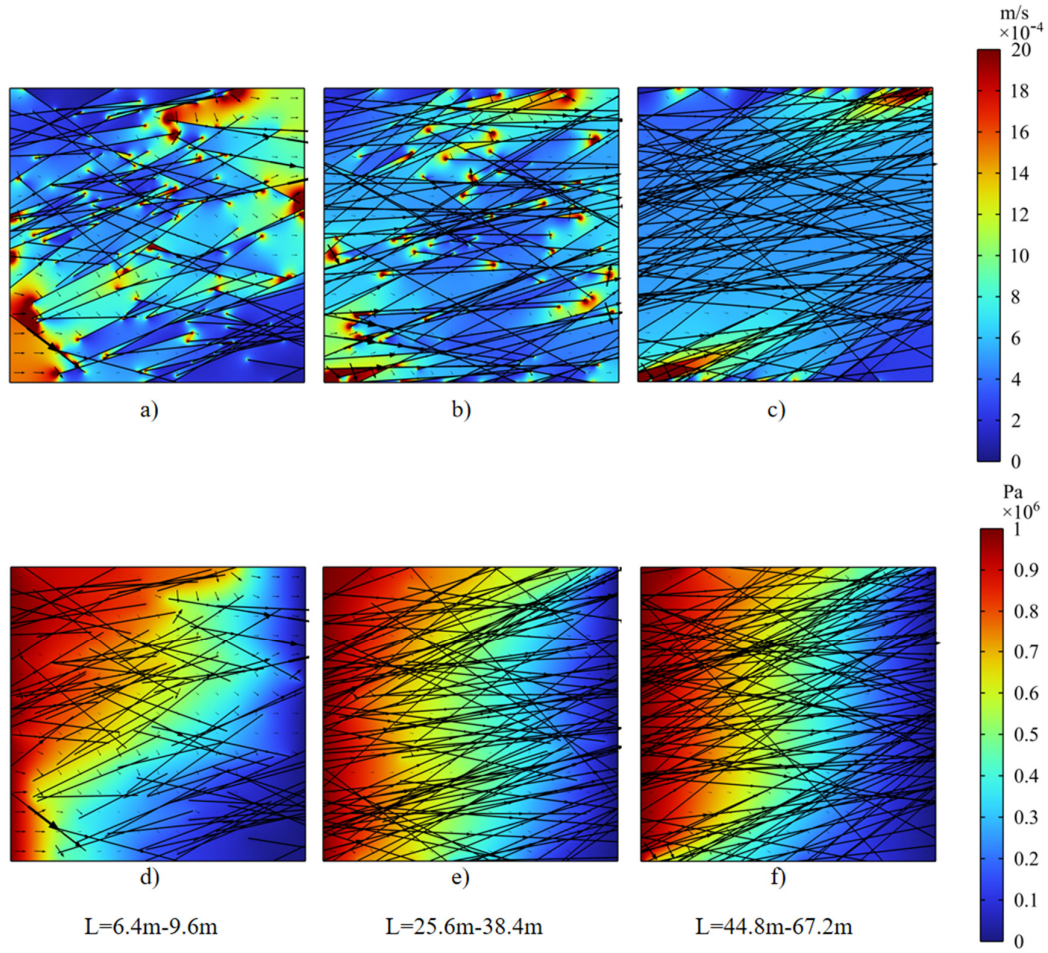
**Table S1.** Random fracture model working condition parameter design.

	Density, /m <sup>2</sup>	Length,m	a <sub>L</sub>	Angle, °	b	Aperture, cm	a <sub>d</sub>
case1	0.25	25.6-38.4	2	45	5	0.08-0.12	2
case2	0.05	25.6-38.4	2	45	5	0.08-0.12	2
case3	0.15	25.6-38.4	2	45	5	0.08-0.12	2
case4	0.35	25.6-38.4	2	45	5	0.08-0.12	2
case5	0.45	25.6-38.4	2	45	5	0.08-0.12	2
case6	0.25	6.4-9.6	2	45	5	0.08-0.12	2
case7	0.25	12.8-19.2	2	45	5	0.08-0.12	2
case8	0.25	19.2-28.8	2	45	5	0.08-0.12	2
case9	0.25	32-48	2	45	5	0.08-0.12	2
case10	0.25	38.4-57.6	2	45	5	0.08-0.12	2
case11	0.25	44.8-67.2	2	45	5	0.08-0.12	2
case12	0.25	25.6-38.4	4	45	5	0.08-0.12	2
case13	0.25	25.6-38.4	6	45	5	0.08-0.12	2
case14	0.25	25.6-38.4	8	45	5	0.08-0.12	2
case15	0.25	25.6-38.4	10	45	5	0.08-0.12	2
case16	0.25	25.6-38.4	2	0	5	0.08-0.12	2
case17	0.25	25.6-38.4	2	15	5	0.08-0.12	2
case18	0.25	25.6-38.4	2	30	5	0.08-0.12	2
case19	0.25	25.6-38.4	2	60	5	0.08-0.12	2
case20	0.25	25.6-38.4	2	75	5	0.08-0.12	2
case21	0.25	25.6-38.4	2	90	5	0.08-0.12	2
case22	0.25	25.6-38.4	2	45	0.1	0.08-0.12	2
case23	0.25	25.6-38.4	2	45	1	0.08-0.12	2
case24	0.25	25.6-38.4	2	45	9	0.08-0.12	2
case25	0.25	25.6-38.4	2	45	13	0.08-0.12	2
case26	0.25	25.6-38.4	2	45	5	0.16-0.24	2
case27	0.25	25.6-38.4	2	45	5	0.24-0.36	2
case28	0.25	25.6-38.4	2	45	5	0.32-0.48	2
case29	0.25	25.6-38.4	2	45	5	0.4-0.6	2
case30	0.25	25.6-38.4	2	45	5	0.08-0.12	4
case31	0.25	25.6-38.4	2	45	5	0.08-0.12	6
case32	0.25	25.6-38.4	2	45	5	0.08-0.12	8
case33	0.25	25.6-38.4	2	45	5	0.08-0.12	10



**Figure S6.** Effect of random fracture density on the flow rate and water pressure

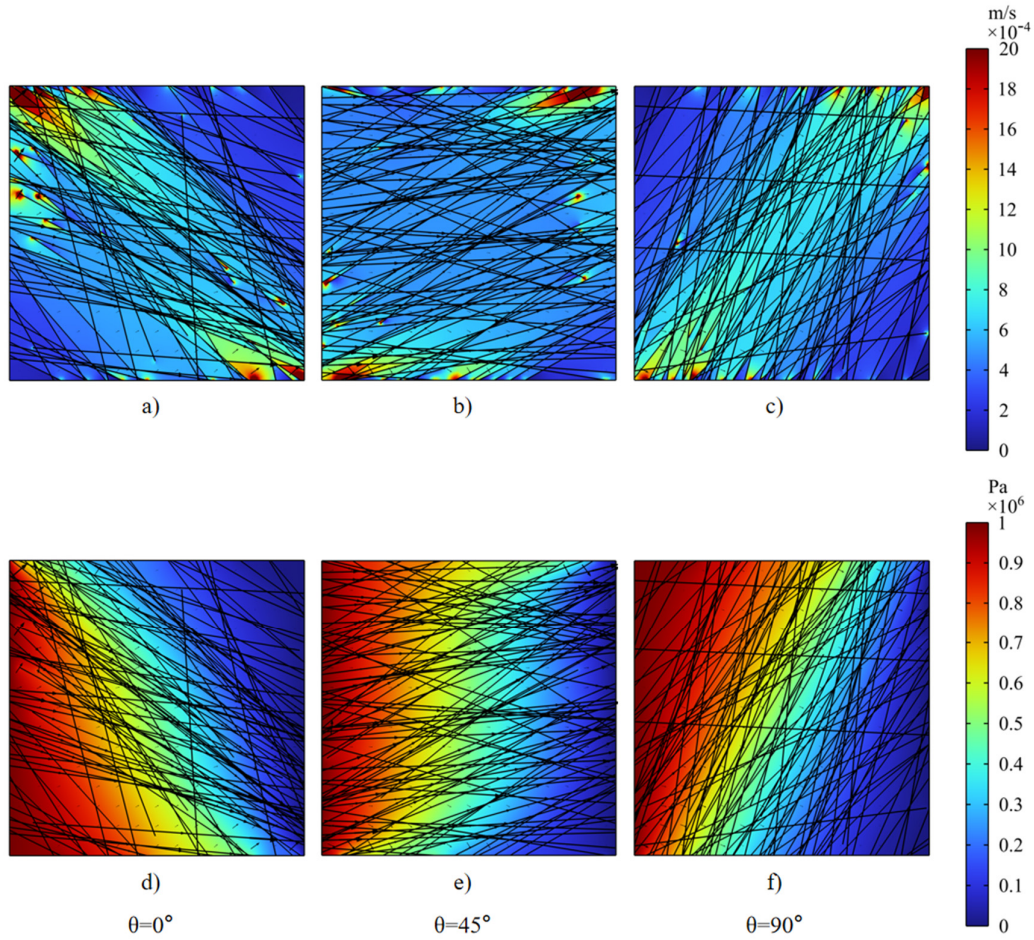
Fracture length variation significantly impacts Darcy's velocity in the rock matrix and pore water pressure distribution. Fig. S7 presents six models examining permeability effects with varying fracture lengths. Models a-c show Darcy's velocity changes with increasing length, while models d-f display pore water pressure variations. As fracture length increases, rock matrix seepage decreases, high hydraulic gradient regions shrink, and fluid transport evolves from fracture-matrix-fracture to fracture-fracture. Pore water pressure variation in models d-f reveals that fracture length influences matrix pressure distribution, particularly in short fractures. Non-linked outlet ends show little pressure variation and uniform distribution, while joint outlet ends have increased water pressure and significant nearby matrix pore pressure changes.



**Figure S7.** Effect of random fracture length on flow rate and water pressure

Changes in fracture angle and dispersion coefficient significantly impact the Darcy's velocity in the rock matrix and the magnitude and distribution of pore water pressure. In Fig. S8, six models examine permeability effects by varying fracture angle while keeping other conditions constant. Models a to c display increased Darcy's velocity with increasing angle, while models d to f show angle variation on pore water pressure. The overall fracture directionality, high hydraulic gradient region location in the matrix, and fluid transport direction change with angle variation. Matrix pore water pressure distribution changes significantly with fracture angle alteration, and overall pressure direction shifts from oblique above to roughly horizontal and eventually oblique right below.

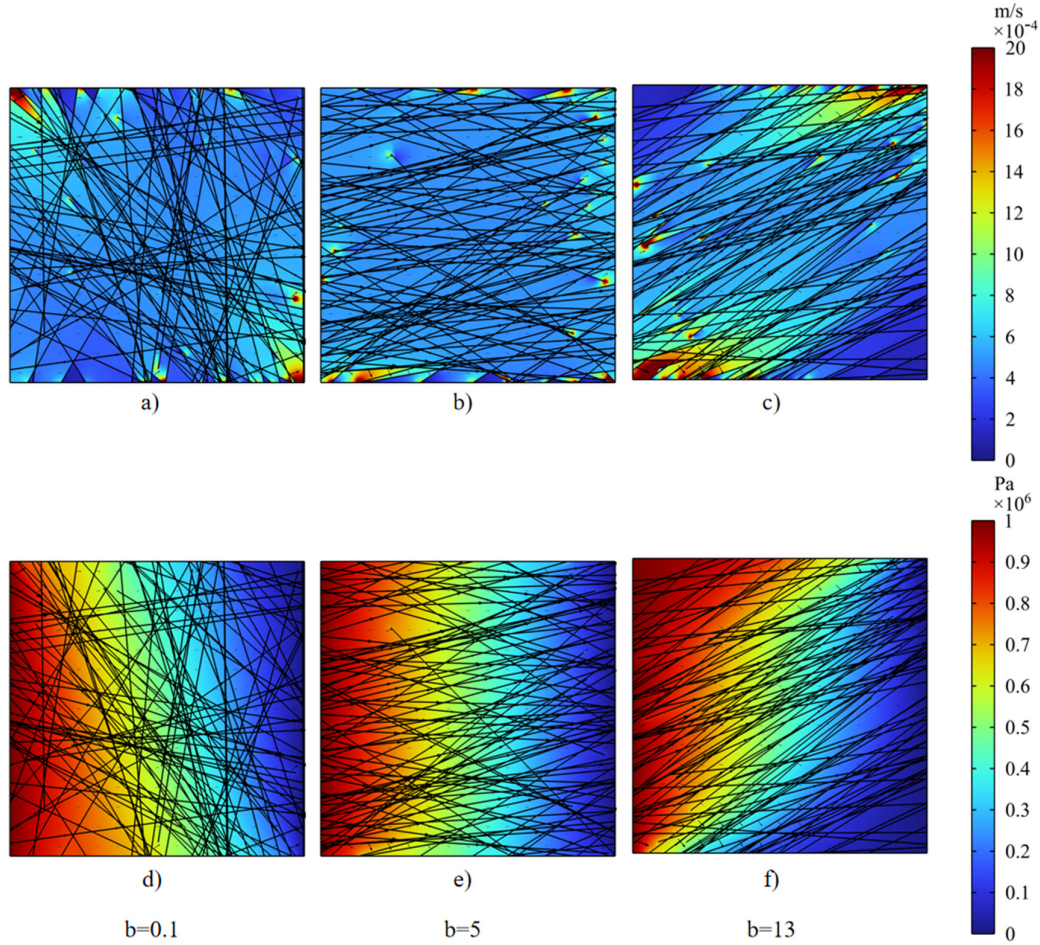




**Figure S8.** Effect of discrete fracture angle on flow rate and water pressure

The six models in Fig. S9 show the impact of the dispersion coefficient on permeability. Models a to c display the variation in Darcy velocity due to increasing dispersion coefficient. Models d to f show the effect of the dispersion coefficient on pore water pressure. It is evident that as the dispersion coefficient increases, the overall deviation angle of the fractures decreases, and more fractures tend to have the same angle. As the dispersion coefficient increases, the seepage direction in the matrix shifts horizontally to the right and gradually tilts to the lower right, and the high hydraulic gradient becomes more concentrated in the upper right and lower left corners of the model from the dispersion. The direction of pore water pressure is the same as the direction of

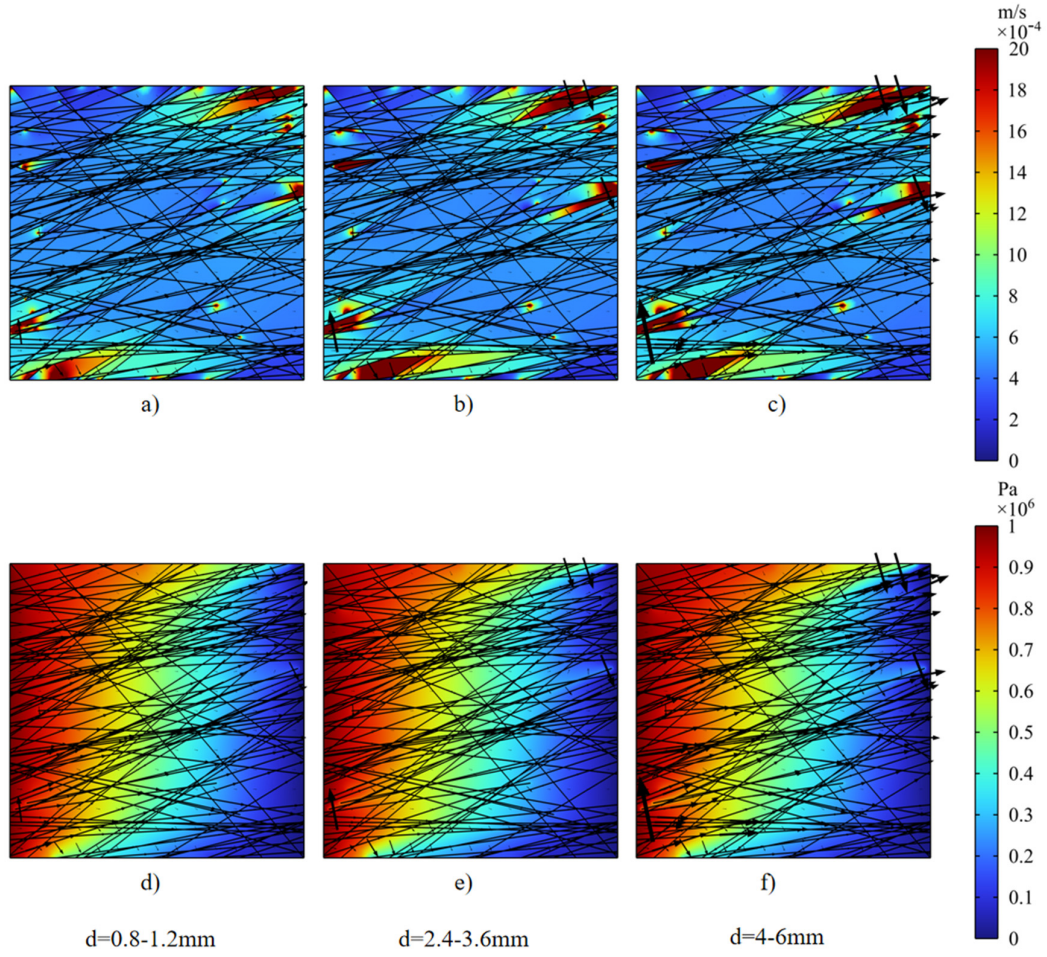
matrix seepage. The direction of the pressure rapid change zone shifts from roughly  $120^\circ$  clockwise to  $90^\circ$ , and finally to  $45^\circ$ .



**Figure S9.** Effect of discrete fracture dispersion coefficient on flow rate and water pressure

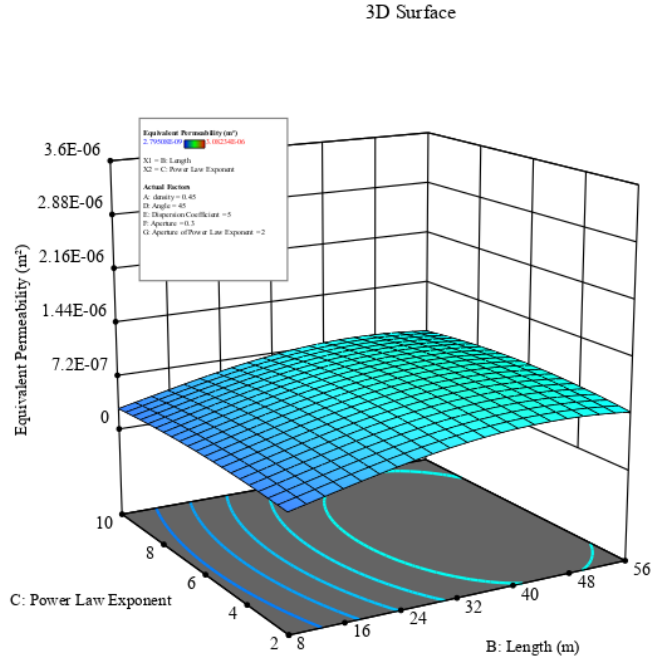
The aperture significantly affects the Darcy velocity and pore water pressure in the rock matrix. In Fig. S10, six models show the impact of varying aperture while keeping other conditions constant. Models a-c display the change in Darcy velocity due to increasing aperture, while models d-f demonstrate the variation in pore water pressure. As the aperture increases, seepage flow in the matrix decreases, seepage flow in the fractures increases significantly, and fluid transport within fractures becomes more pronounced.





**Figure S10.** Effect of random fracture angle on the flow rate

Fig. S11 shows that effect of length and length power law interaction on permeability, and the length power law significantly influences the distribution of fracture length, indirectly affecting permeability. When the length power law was 6, the impact of fracture length on permeability was most pronounced.



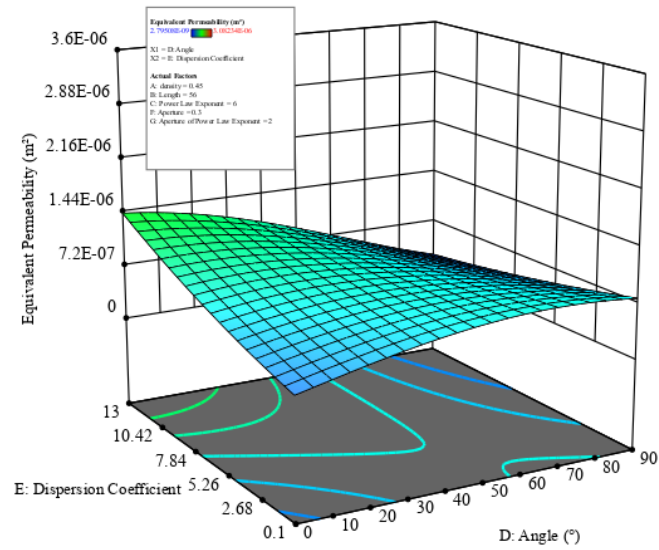
**Figure S11.** Effect of length and length power law interaction on permeability

Fig. S12 presents the effect of angle and dispersion coefficient interaction on permeability.

Fracture angle negatively correlates with permeability, and the deviation angle between fractures indirectly affects the distribution trend of fracture angles. As the dispersion coefficient increases, the deviation angle decreases, while it increases as the dispersion coefficient decreases. When the parameter angle was small, the dispersion coefficient positively correlated with equivalent permeability; when the parameter angle was large, it negatively correlated with equivalent permeability.



### 3D Surface



**Figure S12.** Effect of angle and dispersion coefficient interaction on permeability

Fig. S13 reveals that aperture power law has an insignificant influence on permeability, while aperture significantly impacts permeability, consistent with previous findings.

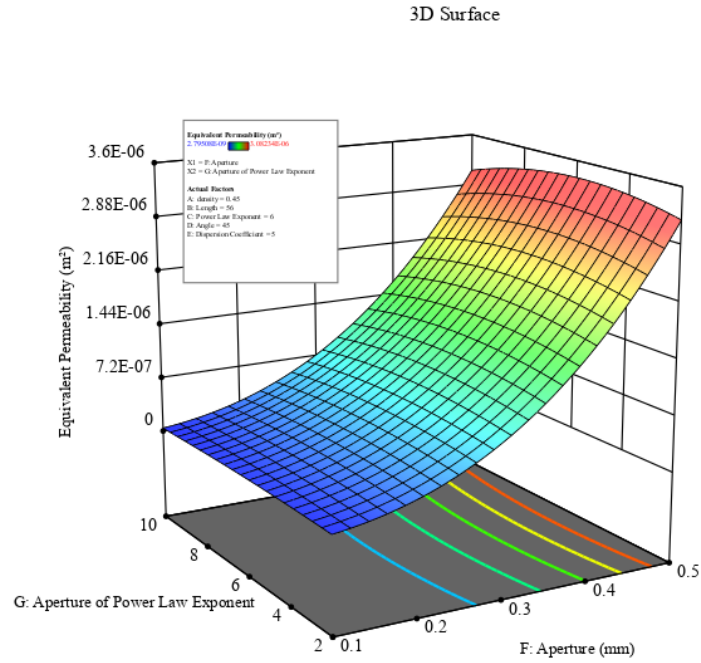


**Figure S13.** Effect of aperture and aperture power law interactions on permeability.

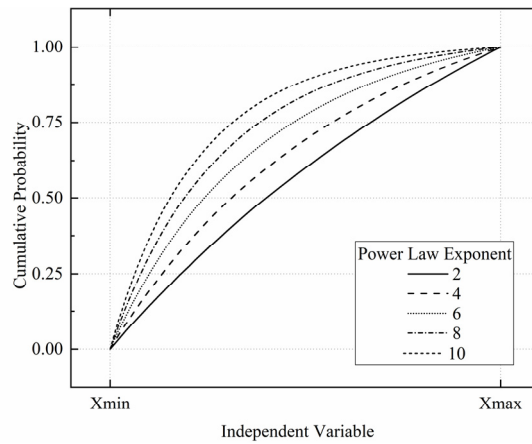


**Figure S14.** Effect of different power law indices on cumulative probability

Figure S14 shows the distribution functions under different power law exponents. In this simulation, the range of  $\pm 20\%$  of the original parameter is chosen as the maximum and minimum value of the design, so  $X_{\max}$  and  $X_{\min}$  is 1.5 at maximum, so the distribution equation under this ratio is chosen.

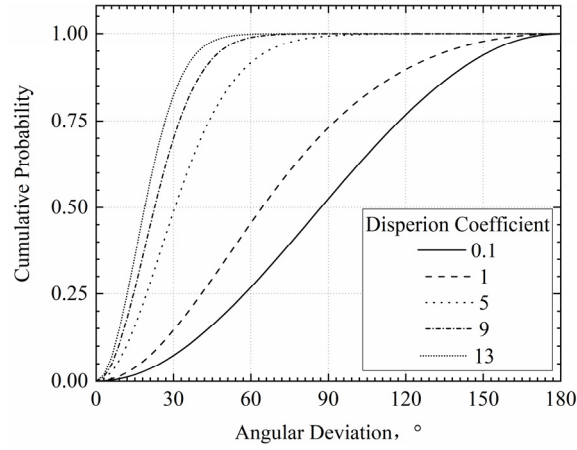


**Figure S15. Effect of different Fisher constants  $K$  on the deviation angle  $\theta$  of the fracture azimuth**

Figure S15 shows the probability distribution under different dispersion coefficients, it can be seen that the deviation angle  $\theta$  decreases with increasing  $K$ . When  $K = 13$ , nearly 75% of the fissure strike deviation angle  $\theta < 30^\circ$ , indicating that the overall variability in fissure strike in the region is not large, while when  $K = 0.1$ , the fissure strike deviation angle  $\theta$  is generally large, some even exceed  $150^\circ$ , which is opposite to the original strike.